The interaction of hydrogen with a cobalt(10$\bar{1}$0) surface

K.-H. Ernst
Swiss Federal Laboratories for Materials Testing and Research (EMPA), Überlandstrasse 129, CH-8600 Dübendorf, Switzerland

E. Schwarz and K. Christmann
Institut für Physikalische und Theoretische Chemie der Freien Universität Berlin, Takustr. 3, D-14195 Berlin, Germany

(Received 22 March 1994; accepted 6 June 1994)

The adsorption of hydrogen on a cobalt(10$\bar{1}$0) surface was investigated in ultrahigh vacuum (UHV) between 85 and 500 K using Video-LEED, temperature-programmed thermal desorption (TPD), work function ($\Delta\Phi$) measurements, and high-resolution electron energy loss spectroscopy (HREELS). Between 90 and 200 K, hydrogen adsorbs dissociatively with high sticking coefficient ($s_0 \geq 0.8$) via precursor kinetics and forms, with increasing exposure, a $c(2\times4)$, a $p2mg$ (2×1) and a (1×2) LEED structure (hydrogen coverages $\Theta_H=0.5$, 1.0, and 1.5, respectively). While the first two structures represent true ordered hydrogen phases there is strong evidence that the (1×2) phase is reconstructed, likely in a paired-row configuration. The formation of the (1×2) phase is slightly thermally activated; its decomposition produces a sharp thermal desorption maximum (α state) appearing on the low-energy side of a β-TPD signal which reflects the hydrogen desorbing from the unreconstructed surface. The activation energies for desorption from the α and β states are 62 and 80 kJ/mol, respectively. Chemisorption in the β state [(2×1) phase up to $\Theta_H=1.0$] is associated with a $\Delta\Phi$ of +207 meV, while the fully developed (1×2) reconstructed phase (α state) causes a $\Delta\Phi$ of approximately −122 meV resulting in an overall work function change of +85 meV at saturation. From HREELS, we determine the H adsorption site in all superstructures to be threefold with a local C_S symmetry. Our results are discussed and compared with previous findings for similar metal–hydrogen interaction systems.

I. INTRODUCTION

During the past decades studies on the interaction of hydrogen with metal surfaces have steadily gained interest, as this kind of interaction plays an often decisive role in practical materials science, physics, heterogeneous catalysis, electrochemistry, and in fuel cell and energy storage technology. While we refer the reader for more general information to various recent review articles on hydrogen adsorption,[1–4] we would like to focus on a particular point here, namely, on the hydrogen-induced restructuring which frequently occurs when hydrogen interacts with metal surfaces. Accordingly, an increasing number of today's studies of hydrogen adsorption on metal surfaces is concerned with phenomena of this kind, whereby both detailed structural analysis (including the uncovered surfaces) and the underlying reconstruction mechanisms are of central interest.

In this article, we report data about hydrogen interaction with a cobalt(10$\bar{1}$0) single crystal surface under ultrahigh vacuum (UHV) conditions. Cobalt plays an important role as a Fischer–Tropsch catalyst;[5] similar to nickel it is very effective in hydrogenation reactions. Quite in contrast to Ni, however, only few studies have been reported on H interaction with Co, dealing in part with polycrystalline films.[6–8] Concerning single crystal studies we mention the early work by Bridge *et al.*[9] and the more recent UV photoemission study by Greuter *et al.*[10] which both dealt with H adsorption on the basal Co(0001) surface. The tendency of the crystallographically more "open" surfaces with (110) (fcc), (211) (bcc), or (10$\bar{1}$0) (hcp) orientation to reconstruct under hydrogen is well known and has recently been reviewed, whereby some preliminary results about the cobalt(10$\bar{1}$0) surface were communicated.[11,12] Here, we present the body of our LEED, TPD, $\Delta\Phi$, and HREELS data; a special report summarizing the angle-resolved UV photoemission (ARUPS) measurements will follow.[13] We concentrate on the H/Co binding energetics and kinetics as well as on the local geometry of the H adsorption sites and long-range order phenomena including the phase transition from the unreconstructed to the reconstructed surface.

II. EXPERIMENT

The experiments were performed in a ~100 L stainless steel UHV chamber equipped with facilities for low-energy electron diffraction (Video-LEED), Auger electron spectroscopy (AES), work function change ($\Delta\Phi$) measurements (Kelvin probe), temperature programmed thermal desorption (TPD) using a differentially pumped quadrupole mass filter, and high-resolution electron energy loss spectroscopy (HREELS). Further instrumental details can be found in a previous publication.[11] The sample consisted of a disk-shaped slab of approximately 10 mm diameter and 2 mm thickness cut by spark erosion from a bulk Co single crystal of 5*N* purity (Lamprecht, Neuhausen Germany) parallel to the (10$\bar{1}$0) plane to within 0.5 deg after appropriate Laue x-ray orientation. The surface was mechanically and electrochemically polished following a procedure described by Welz *et al.*[14] The crystal was then gently spot-welded between two parallel-running tantalum wires which, in turn, were clamped between massive copper rods attached to a long z-travel manipulator. The sample could be resistively

 0021-9606/94/101(6)/5388/14/$6.00

heated to 700 K and (via the Cu rods) liquid–nitrogen cooled to about 85 K. The temperature T was measured by a chromel–alumel thermocouple and controlled by a special regulator and ramp generator.[15] Initially, AES revealed heavy C, S, and O surface contaminations. Cleaning was achieved by prolonged argon ion bombardment (500 eV, 36 mA cm^{-2}), whereby T was slowly increased to 500 K. It is worth mentioning here that [hexagonal-close-packed (hcp)] α-cobalt undergoes a phase transition to the [face-centered-cubic (fcc)] β form around 693 K,[16] and it is essential for maintaining a well-ordered single crystal surface not to exceed this transition temperature. All in all, carbon was the most persistent contamination; fortunately, it readily segregates on the surface at elevated temperatures and can be effectively depleted by Ar sputtering. Final C traces can be removed by a gentle oxygen treatment at 650 K (oxygen pressure $\approx 10^{-8}$ mbar for short intervals), whereby small oxygen exposures are vital in order not to oxidize the Co surface. Admission of the gases (Ar, O_2, H_2) to the chamber was accomplished by bakeable stainless steel leak valves (Varian); total gas pressures were measured by a Bayard–Alpert ion gauge. All pressure and exposure values given in this work have been corrected with the respective gauge sensitivity factors. Video-LEED measurements were performed using the equipment and procedure developed at the University of Erlangen.[17] The HREELS data were obtained utilizing an instrument developed and designed by Unwin *et al.*[18] In specular measurements, the angle of incidence of the electrons was 50 deg (all angles here are given with respect to the surface normal). The primary electron beam energy could be varied between 1 and 10 eV with typical resolutions between 10 and 13 meV [full width at half-maximum (FWHM)] and elastic peak count rates of about 50 000 counts/s. Off-specular measurements were carried out at constant angle of incidence, but with variable collection angle. To find a favorable primary beam energy for acquiring off-specular spectra, we monitored the intensity of the elastic beam under specular conditions while varying the beam energy. Only with H adsorbed on the surface, the resulting "reflectivity curve" showed at 4.5 eV a significant intensity minimum. According to Conrad *et al.*,[19] the cross section for exciting H surface vibrations exhibits a maximum when the primary energy is adjusted to reveal a minimum of the reflectivity curve. This effect was indeed confirmed also in the present study. All HREEL spectra were recorded along the two symmetric azimuthal directions ([0001] and [$1\bar{2}10$]) at a temperature of ~90 K.

III. RESULTS

A. LEED

A short remark concerns the structure of the clean hcp ($10\bar{1}0$) surface. Similar to the fcc (110) face, it is of twofold symmetry and exhibits troughs and close-packed rows of atoms along [$1\bar{2}10$] and periodically interrupted rows in the [0001] direction. Depending on which surface layer (A or B) of the stacking sequence A...B...A of the hcp lattice is the terminating surface, the hcp ($10\bar{1}0$) face can exhibit two different configurations which are illustrated in Fig. 1. The

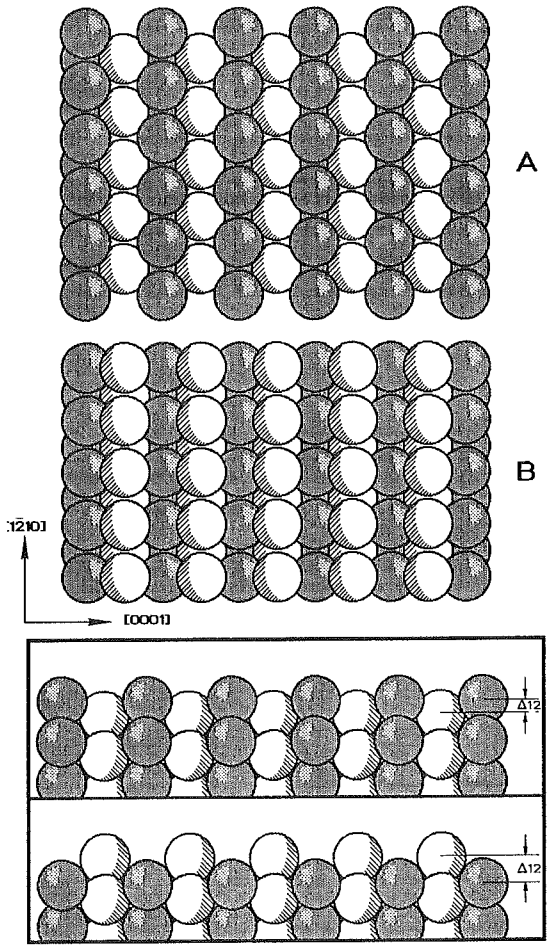

FIG. 1. The hcp($10\bar{1}0$) face can theoretically exist in two different modifications: A and B. In the case of cobalt, the less corrugated form A was confirmed by LEED (Refs. 20 and 21).

structures "A" and "B" differ with respect to the second layer distance Δ_{12}: in configuration "A," Δ_{12} is only 0.72 Å, while in "B" Δ_{12} is twice as large, namely 1.442 Å. In addition, the first and second layer atoms are collinear only in termination "B." We took, in a separate study, LEED intensity-voltage (I,V) curves from the clean Co($10\bar{1}0$) surface and performed dynamical LEED calculations[20] which confirmed the less corrugated configuration "A," in agreement with a study independently performed by Lindroos *et al.*[21]

After appropriate cleaning and prolonged annealing, the Co($10\bar{1}0$) sample showed a LEED pattern with bright and fairly sharp diffraction spots on a low background indicative of a chemically clean and well-ordered surface [Fig. 2(a)].

1. Commensurate hydrogen phases: The c(2×4) and the (2×1)p2mg structures

Exposure to hydrogen gas at $T \approx 90$ K gives rise to three ordered LEED superstructures. After a dose of 2.3×10^{-5} Pa s (0.17 L) at 90 K, weak "streaks" appear parallel to the $\mathbf{a}_1^*$ vector at the $\pm n/2$ positions ($n=0, 1, 2, 3,...$) of $\mathbf{a}_2^*$ [see Fig. 2(b)]. With further exposure to H_2 the streaks coalesce

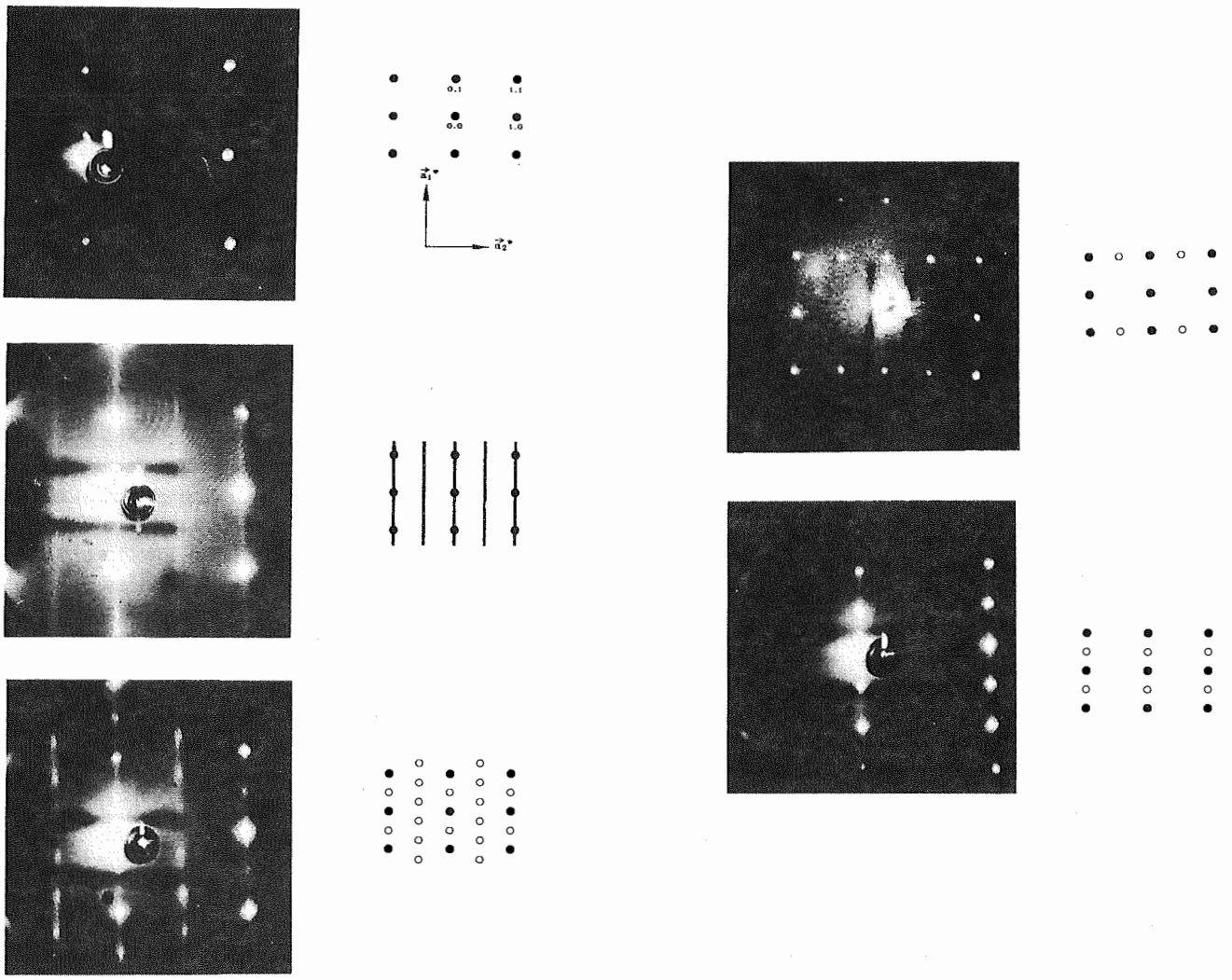

FIG. 2. LEED photographs of (a) the clean Co(10$\bar{1}$0) surface (Ep=66 eV), (b) the "streak" $c(2\times4)$ precursor phase (Ep=64 eV), (c) the $c(2\times4)$ 4H structure (Ep=52 eV), (d) the $p2mg(2\times1)$ 2H structure (Ep=60 eV), and (e) the (1×2) 3H structure (Ep=63 eV).

to spots of a $c(2\times4)$ structure [Fig. 2(c)] which reach their maximum in intensity after a dose of 3.8×10^{-5} Pa s (0.28 L). With increasing exposure the fractional-order beams transform to a sharp (2×1) structure which reaches maximum intensity after approximately 1.2×10^{-4} Pa s (0.9 L) [see Fig. 2(d)]. In the respective (2×1) LEED pattern all $(\pm n/2, 0)$ spots (n=1,2,...) are missing, when the plane of electron incidence is parallel to the [1$\bar{2}$10] azimuth. This observation indicates a glide mirror plane along [1$\bar{2}$10][22] and requires a unit cell containing two H atoms located in identical adsorption sites. Similar structures were previously reported for H adsorption on Pd(110) and Ni(110).[23–26] Accordingly, the total hydrogen atom coverage in this (2×1) phase amounts to Θ_H=1 ($\cong9.8\times10^{14}$ atoms cm^{-2}) which can be used as a coverage standard for all other H coverages (see Sec. III B). A distinction between the two possible space groups $p1g1$ or $p2mg$ is possible by considering the HREELS results (cf. Sec. III D) which suggest, for all H superstructures, an identical local C_S symmetry of the individual H–Co adsorbate complexes with respect to the [0001] azimuth. This finding can only be reconciled with the $p2mg$ space group of the two-dimensional lattice. It must be added here that the intensity of the "extra" spots in all the structures described so far is very small, about 1%–10% of the Co(1×1) spot intensity. This is the expected result, since H atoms (even in the adsorbed state) are known to scatter low-energy electrons very ineffectively, and we may take this result as evidence that these phases do not involve significant Co surface reconstruction effects.

2. Reconstructed phases: The (1×2) structure

Continuous hydrogen exposure causes the slow appearance of a (1×2) superstructure [Fig. 2(e)] which coexists with the $(2\times1)p2mg$ phase over quite a range of exposures. This coexistence is indicative of a first-order phase transformation, in which (1×2) islands grow within a "sea" and at the expense of (2×1) arrays. There are two other important observations, namely (i) that the H exposure necessary to reach the (1×2) intensity maximum depends strongly on the

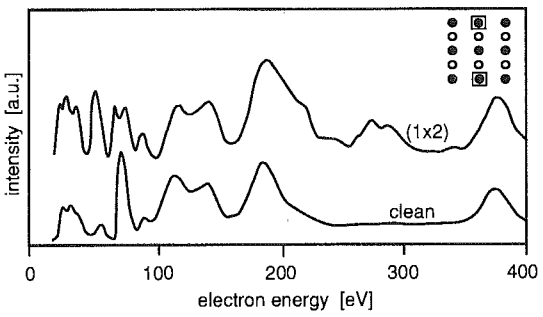

FIG. 3. I/V curves of the (0,1) LEED beam of the clean Co(10$\bar{1}$0) surface and the (1×2) 3H structure, respectively. The strong differences between these curves cannot be explained by a "true" hydrogen superstructure; therefore, a reconstruction is very likely.

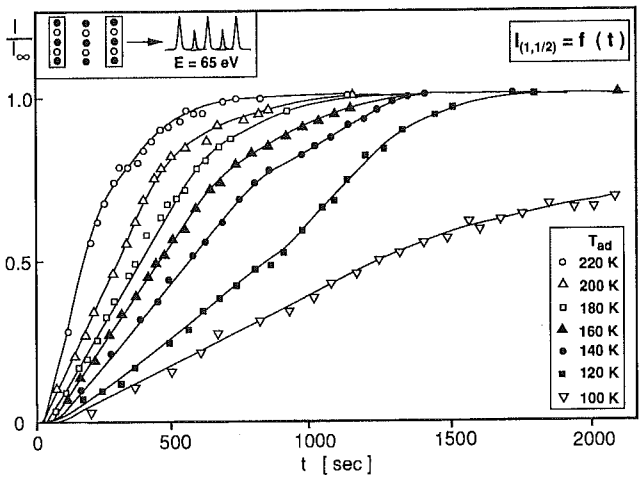

FIG. 4. Intensity of the $(1\frac{1}{2})$ fractional-order beams (determined from the beam profile areas) vs hydrogen exposure time ($P_{H_2} = 1.6 \times 10^{-7}$ mbar), for seven different temperatures. The integral intensity was normalized with respect to the saturation intensity (I_∞) at the respective temperature.

temperature of the Co sample and (ii) that the intensity of the fractional-order beams of the (1×2) structure is comparable to that of the integer-order beams. Taken together, we conclude from this that the (1×2) structure involves a pronounced reconstruction of the Co substrate, whose development is kinetically limited. This conclusion is quite in line with the strong alteration of the LEED intensity vs voltage (I,V) curves displayed in Fig. 3. This figure compares the integer-order (0,1) beam of the clean (1×1) surface and the hydrogen-induced (1×2) structure. The differences between both curves cannot be explained by the additional scattering of electrons from H atoms; rather, the maxima occurring in the "(1×2)" curve (especially around 300 eV beam energy) are indicative of a displacement of Co surface atoms caused by chemisorption of hydrogen.

Concerning the temperature dependence of the H-induced LEED structures we state that all ordered phases except the (1×2) exhibit the common order–disorder phase transition behavior, that is to say, the order disappears at higher temperatures and reappears reversibly at lower temperatures. We determined the following order–disorder transition temperatures T_{crit}: streak phase ≈100 K, $c(2\times4)$≈120 K, and (2×1) $p2mg$ phase ≈170 K. Strikingly different, however, is the temperature dependence of the (1×2) phase. This phase disappears irreversibly as the surface is heated to just beyond 230 K. Thermal desorption experiments (cf. Sec. III B) show that the removal of the (1×2) phase is associated with a partial thermal desorption of adsorbed hydrogen. If a Co surface that was treated in this way and suffered a partial loss of hydrogen is cooled to below 170 K the $p2mg(2\times1)$ phase reappears. We may, therefore, conclude that the desorptive loss of hydrogen involves only the population of the (1×2) phase.

We return to the interesting temperature dependence of the formation of the (1×2) structure which is demonstrated by means of Fig. 4: plotted therein is the fractional-order LEED intensity of a $(1,\frac{1}{2})$ beam (at 65 eV electron energy) against the hydrogen exposure, for different Co crystal temperatures T. Note that only the exposure time was varied, while the H_2 pressure was kept constant at 1.6×10^{-7} mbar. The crystal temperature was varied between 100 and 220 K (which was the ultimate temperature at which thermal desorption of H_2 was still negligible). The LEED intensity was determined by integrating over four symmetry-equivalent fractional-order beams. Due to the increasing thermal broadening and thermal diffuse scattering at elevated temperatures the profiles were normalized with respect to the saturation intensity (I_∞) obtained at the respective temperature. Clearly, the slope of the curves [which reflects the rate of formation of the (1×2) phase] increases with increasing T_{ad} thus pointing to an activation barrier for the (1×2) phase to form (a process which includes both the H adsorption and the displacement of Co surface atoms). Accordingly, we have, in Fig. 5, plotted the logarithm of the initial slope (=rate) vs the inverse temperature. The slope of this Arrhenius plot reveals an apparent activation energy of 2.5 (±0.8) kJ/mol.

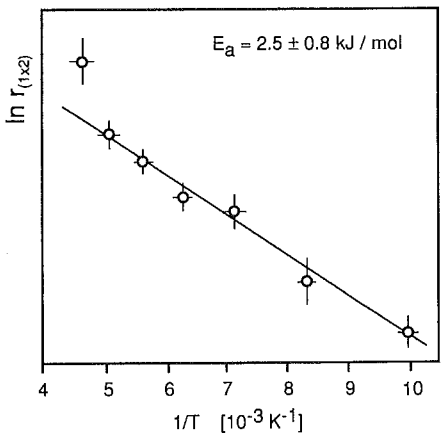

FIG. 5. Arrhenius plot for the formation rates of the (1×2) structure (i.e., initial slope of the curves of Fig. 4) and the respective crystal temperatures. The slope of the straight line reveals an activation energy of ~2.5 (±0.8) kJ/mol.

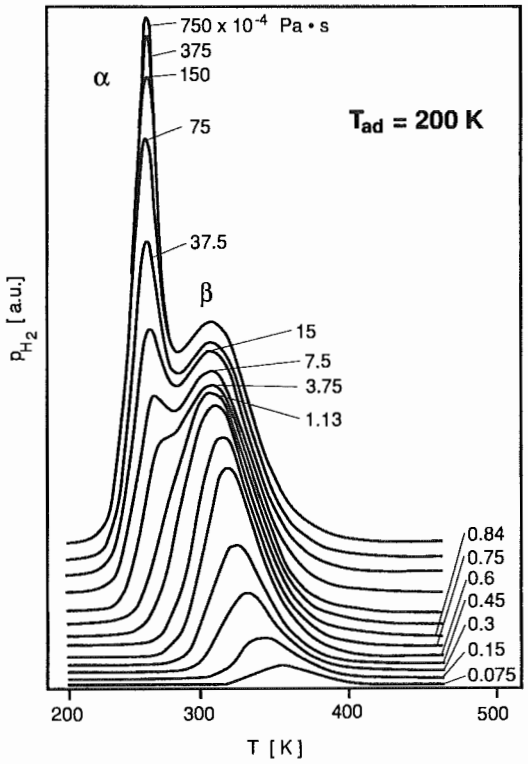

FIG. 6. Series of TPD spectra, taken after different hydrogen exposures (indicated) at an adsorption temperature of T_{ad}=200 K. The two desorption states are denoted as α and β. The heating rate dT/dt was 20.5 K/s.

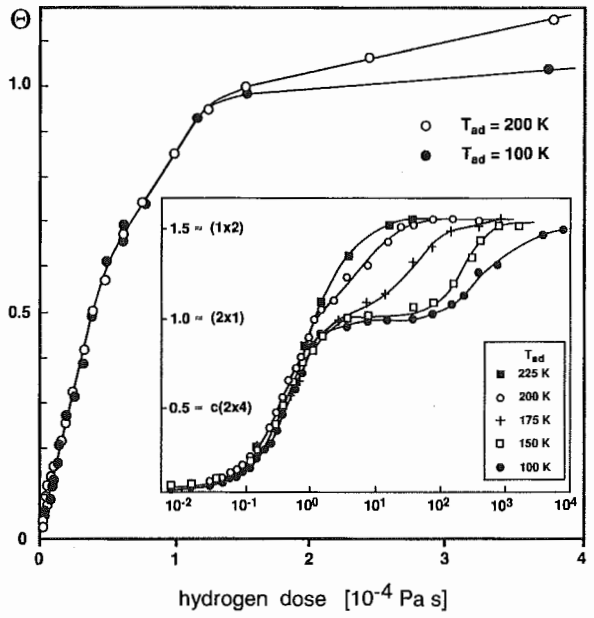

FIG. 7. Coverage-exposure function for hydrogen adsorption on Co(10$\bar{1}$0) at two temperatures (100 K: full circles; 200 K: open circles). The absolute coverage was determined from LEED (see the text). The inset shows the same function for a much larger range of exposures and for additional temperatures. For coverages below one monolayer, the Θ exposure function is independent of the crystal temperature; above Θ_H=1, it clearly depends on T.

B. Temperature-programmed thermal desorption (TPD)

Figure 6 shows a series of thermal desorption spectra obtained after dosing increasing amounts of hydrogen gas at T_{ad}=200 K and taken with a heating rate β=20.5 K/s. Two desorption states can be distinguished, denoted as α and β, whereby the β state develops first and is nearly completed after an exposure of $\sim 1.5\times10^{-4}$ Pa s ($\sim$1.1 L). Then the α state begins to develop on the low-temperature tail of the β state. The α state is much narrower (FWHM: 20 K) than the β state (FWHM: 80 K). The desorption maximum of the β state shifts with increasing coverage to lower temperatures indicating a second-order rate process in which the recombination of two individual H atoms is rate-limiting. This behavior (as well as separate hydrogen–deuterium isotope exchange experiments) unambiguously confirm the atomic nature of the hydrogen chemisorption under these conditions—as it is regularly observed with transition metal surfaces. A second-order Redhead plot assuming a coverage-independent activation energy for desorption (for more details, see Ref. 29) reveals a straight line whose slope can be evaluated to yield an activation energy for desorption of $E^*_\beta \approx 75.5$ kJ/mol. The TPD traces of Fig. 6 were also subjected to a line shape analysis[27,28] which allowed conclusions to be made on the coverage dependence of E^*_β: up to Θ_H=0.5 E^*_β remained approximately constant at 85 ($\pm$15) kJ/mol. [The hydrogen coverages were calibrated using the TPD spectrum of the fully developed $(2\times1)p2mg$ phase as a reference for Θ_H=1.0.] In contrast to the β state the desorption temperature of the α state is invariant with Θ_H suggesting a first-order desorption kinetics.[29] Assuming a frequency factor of $\nu_1=10^{13}$ s^{-1} we deduce an activation energy $E^*_\alpha \approx 62$ kJ/mol. As compared to the β state, fairly massive H_2 exposures are required to fill the α state; it is saturated near a coverage of Θ_H=1.5 monolayers. Quite interestingly the population of the α state depends strongly on the adsorption temperature T_{ad}: the lower T_{ad} the higher the exposure to fill the α state. To give an example, we need about 7.5×10^{-1} Pa s ($\sim$5600 L) to saturate α at 100 K, but only about 7.5×10^{-2} Pa s ($\sim$560 L) to reach the same level of saturation at 200 K. We note that the filling of the β state is comparatively little influenced by T_{ad} as long as this temperature is sufficiently far away from the desorption maximum. In terms of the hydrogen sticking probability **s** we may state that **s** remains T-independent (at least in the range 100 K$<T_{ad}<$200 K) up to approximately one monolayer (Θ_H=1); at higher coverages, however, a significant T dependence of **s** becomes apparent leading to the interesting case that higher temperatures cause a higher sticking probability of hydrogen. We have integrated various TPD curves and plotted the area $\int P\,dt \sim \Theta_H$ vs the exposure; the result is displayed in Fig. 7. In order to underline the influence of T_{ad} on **s** we have included an inset showing a semilogarithmic plot for five temperatures between 100 and 200 K. The slope of these curves directly yields the sticking probability **s** as a function of the hydrogen coverage. Independent of T_{ad}, the sticking coefficient is constant up to Θ_H=0.5 [$c(2\times4)$ phase]; then it drops markedly to about half its initial value, reaches a small plateau between 0.6$<\Theta_H<$1.0, and then

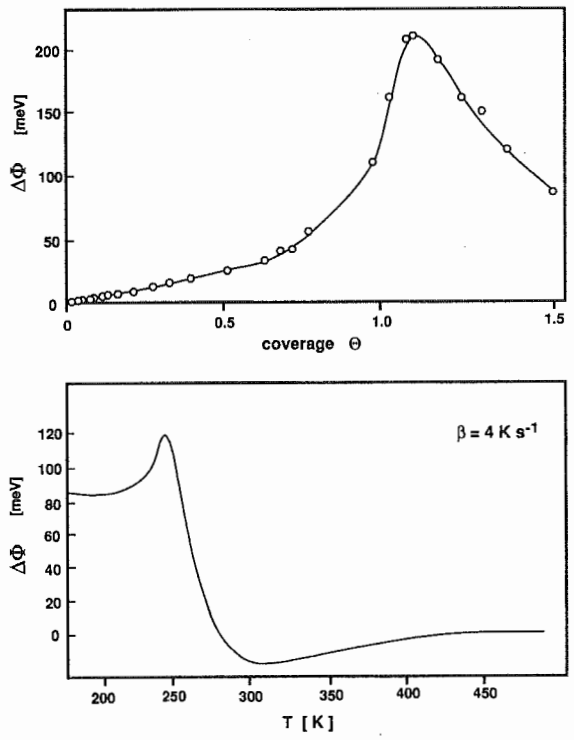

FIG. 8. (a) H-induced work function change $\Delta\Phi$ vs hydrogen coverage Θ_H. This curve was obtained from a continuous $\Delta\Phi$ measurement during H_2 exposure with the coverage calibrated according to Fig. 7. Note the linear initial increase, the abrupt change of the slope around $\Theta_H \approx 0.6$, and the sharp maximum near the monolayer coverage! (b) Temperature dependence of the H-induced work function change [measured during the desorption of hydrogen from Co(10$\bar{1}$0) at a rate of $dT/dt = 4$ K/s]. The $\Delta\Phi$ increase around 240 K is caused by the lifting of the reconstruction and the simultaneous desorption of the hydrogen α state, whereas the subsequent $\Delta\Phi$ decrease is due to hydrogen desorption from the β state.

drops to very small values as Θ_H exceeds 1.0, i.e., when the (1×2) reconstructed phase is formed. Making use of our absolute coverage calibration we can also calculate the absolute value of the initial sticking probability for H_2 on Co(10$\bar{1}$0) to be approximately 0.76 (±25%) (which is in the expected range for a crystallographically open surface).[4] It is very suggestive to correlate the population of the α state with the H-induced surface reconstruction; as will be pointed out in Sec. IV, we have the interesting situation here that the thermally activated formation of a certain substrate surface structure provides additional adsorption sites for hydrogen which fully explains the unusual behavior of increasing sticking with increasing temperature.

C. Work function ($\Delta\Phi$) measurements

Figure 8(a) shows the change of the work function with increasing H coverage, for an adsorption temperature of $T_{ad} = 200$ K. The curve was derived from a direct measurement of $\Delta\Phi$ as a function of H_2 exposure (cf. Ref. 11), whereby the exposure scale was transformed to absolute coverages via the calibrated TPD peak areas. At small coverages there is a practically linear increase of $\Delta\Phi$ with coverage which extends up to $\Theta_H \approx 0.6$. This coverage corresponds to the fully developed $c(2\times4)$ LEED structure; as the $(2\times1)p2mg$ phase starts to form, we observe a marked positive curvature of $\Delta\Phi(\Theta)$ which reaches a relatively sharp maximum of ~207 meV around $\Theta_H = 1$ coinciding with the (2×1) LEED phase intensity maximum. The maximum is then followed by a continuous decrease of $\Delta\Phi$ as the reconstructed (1×2) phase develops, and the $\Delta\Phi(\Theta)$ curve reaches a saturation value of ≈85 meV at a coverage of 1.5. For the initial linear part of the $\Delta\Phi(\Theta)$ curve, we may neglect depolarization effects and apply the simple Helmholtz equation in order to derive the initial dipole moment of the individual H–Co adsorption complex μ_0. μ_0 turns out to be comparatively small, namely 0.014 D. In order to check the reversibility of the H adsorption we prepared the H-saturated surface at 100 K and performed a slow thermal desorption experiment (heating rate = 4 K s^{-1}), while the work function change was simultaneously recorded [Fig. 8(b)]. The respective curve allows us to delineate between the α state, cf. Sec. III B (which desorbs between 200 and 240 K), and the β state which desorbs between 240 and 300 K. If we compare Figs. 8(a) and 8(b) we can easily identify the work function contributions of the α and β state: The α state is apparently associated with a decrease of $\Delta\Phi$ (as Φ *rises* when α desorbs), while the β state causes an *increase* of $\Delta\Phi$ (as Φ *drops* when β desorbs). The slight increase of $\Delta\Phi$ in the temperature range beyond 320 K is difficult to interpret as it may either reflect a small adsorptive contribution on step sites or simply reflect a temperature dependence of the work function of the clean Co surface. A comparison between Figs. 8(a) and 8(b) reveals further that the absolute work function change due to the population of the β state is in the range between 100 and 120 meV; if we attempt to extract the same information for the α state we immediately realize that the $\Delta\Phi$ maximum in the $\Delta\Phi(T)$ curve of Fig. 8(b) reaches only 120 meV and not 207 meV as it does during the *adsorption* run—an unexpected situation for a completely reversible cycle. The reason for this irreversibility here is that the adsorption/desorption equilibrium is not really established during the $\Delta\Phi$ heating experiment; H atoms are increasingly lost as the (1×2) reconstructed surface decomposes and there are different coexistence conditions between patches of (1×2) and (2×1) around 250 K (i.e., during the heating experiment) than around 100 K (where the *adsorption* experiment was performed). Furthermore, as the hydrogen adsorption/desorption for H coverages beyond 1.5 is always accompanied by a (T-dependent) displacement of surface atoms (surface reconstruction) which likewise alters the surface potential and causes a work function change in addition to the dipole moments arising from the H–Co complexes it is impossible to disentangle the respective work function contributions. As a consequence, the H-induced $\Delta\Phi$ can be used as an unambiguous coverage monitor only for $\Theta_H < 1.0$, where the reconstruction effects are absent. However, in the submonolayer range, a given $\Delta\Phi$ value corresponds to a certain H coverage, and the $\Delta\Phi$ signal can be used to monitor the H coverage as a function of temperature and equilibrium gas pressure. In close analogy to previous thermodynamic work[30] $\Delta\Phi$ ($\sim\Theta_H$) can be followed as a function of the hydrogen gas pressure for a given constant sample temperature T (isotherms). The respective plot is shown in Fig. 9. Making

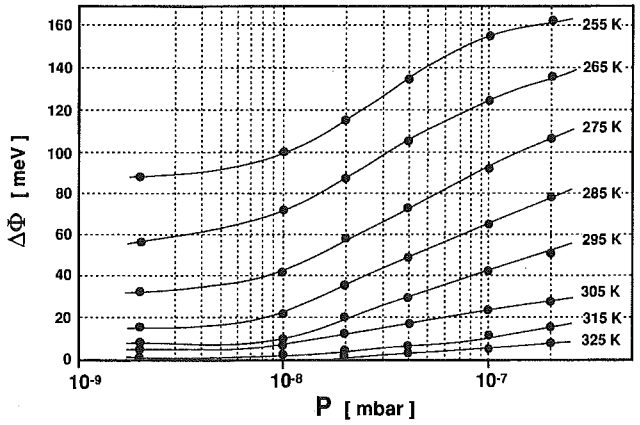

FIG. 9. Series of adsorption isotherms for hydrogen on Co(10$\bar{1}$0), whereby the adsorbate concentration was monitored by the H-induced work function change $\Delta\Phi$.

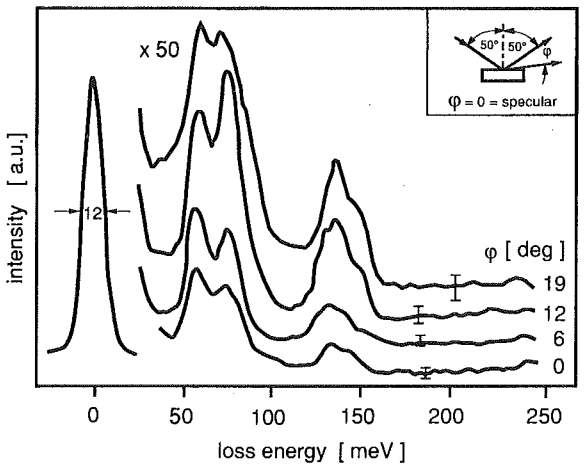

FIG. 10. Vibrational loss spectrum (Ep=4.5 eV) of hydrogen adsorbed in the $c(2\times4)$ phase ($\Theta_H\approx0.5$ at 100 K) with the scattering/detection plane oriented along the [0001] azimuth [perpendicular to the troughs of the (10$\bar{1}$0) surface]. The incidence angle was 50°; the detection angle varied from 50° (specular direction, bottom curve) up to 69° (=19° off-specular, top curve).

use of the Clausius–Clapeyron equation for the equilibrium: gas phase–adsorbate phase, Arrhenius-type of plots ($\ln P$ vs $1/T$) for constant coverage yield the isosteric heat of adsorption, q_{st}, as a function of hydrogen coverage Θ_H. It turns out for the present system that q_{st} amounts to ~80 kJ/mol, fairly independent of the hydrogen coverage up to Θ_H=1.0, in close agreement with the result of the TPD analysis (cf. Sec. III B). No further attempt was made to derive, e.g., the adsorption entropy; as the isosters cover a fairly wide temperature range from 100 up to 325 K the degree of long-range order within the adsorbate layer varies from very good order (verified at low temperatures, i.e., high coverages) to disorder (verified at high temperatures, i.e., small coverages), and clues on the configurational entropy of the adsorbate are difficult to obtain.

D. High-resolution electron energy loss spectroscopy (HREELS)

It is well-known that vibrational loss spectra are very helpful for acquiring information on the local coordination geometry and symmetry of the H atoms in their adsorption sites on the Co surface. In this respect, most of the different LEED phases described in Sec. III A exhibit different HREEL spectra, and this section is organized in a way that the HREELS features of the various ordered hydrogen phases are described as they develop with increasing hydrogen coverage.

1. HREELS for Θ_H<1 ML: The c(2×4) phase

Figure 10 shows a typical vibrational loss spectrum taken at $\Theta_H\approx0.5$ and 100 K [where the $c(2\times4)$ phase is fully developed], with the scattering/detection plane oriented along the [0001] azimuth [perpendicular to the troughs of the (10$\bar{1}$0) surface]. The relatively high noise level of the spectrum is caused by the fact that the sticking probability of hydrogen is very high under the experimental conditions, and even at ambient pressures below 10^{-10} mbar (where H_2 is the main component) there is only a small coverage window in which the pure $c(2\times4)$ phase is stable. Therefore, the energy scans had to be performed at high scan rates. Furthermore, the inherent signal intensity of the H losses, particularly in the $c(2\times4)$ structure, is very low—this is the reason why we chose a relatively low resolution of our HREELS instrument (FWHM>12 meV) which prevented us from detecting further weak losses which possibly appear. The "streak" phase showed almost identical loss features as the $c(2\times4)$ structure, but with even lower intensities. This behavior suggests that the streak phase may be regarded as a real precursor of the $c(2\times4)$ hydrogen phase, however, with less pronounced long-range order in one dimension. In the spectrum displayed in Fig. 10, clearly four H-induced dipole-active losses at 58, 75, 135, and 145 MeV can be distinguished whose intensities decrease as the off-specular angle increases. As pointed out in Sec. IV, this high number of losses demands at least two different types of hydrogen adsorption sites. Furthermore, the observed intensity ratios of all the losses exclude that the peaks at higher energies are due to overtones. Two loss energies are very similar to those of the (2×1) structure (see below), which suggests that one of the H sites is identical with the respective site in the (2×1) structure. Although the four losses mentioned above appear more clearly in the [0001] azimuth, they can also be distinguished in the perpendicular [1$\bar{2}$10] direction, however, with a somewhat worse signal-to-noise ratio which leaves the possibility open that still more losses are hidden in the tail of the main vibrational bands (a slight asymmetry may be taken as a respective hint).

2. HREELS for Θ_H<1 ML: The (2×1) phase

Figure 11(a) shows a typical vibrational loss spectrum which we obtained in the specular direction with the scattering plane directed parallel to the [1$\bar{2}$10] azimuth, i.e., along the troughs of the (10$\bar{1}$0) surface. The temperature was again ~100 K and the hydrogen coverage was adjusted close to one monolayer so that the $(2\times1)p2mg$ phase was fully de-

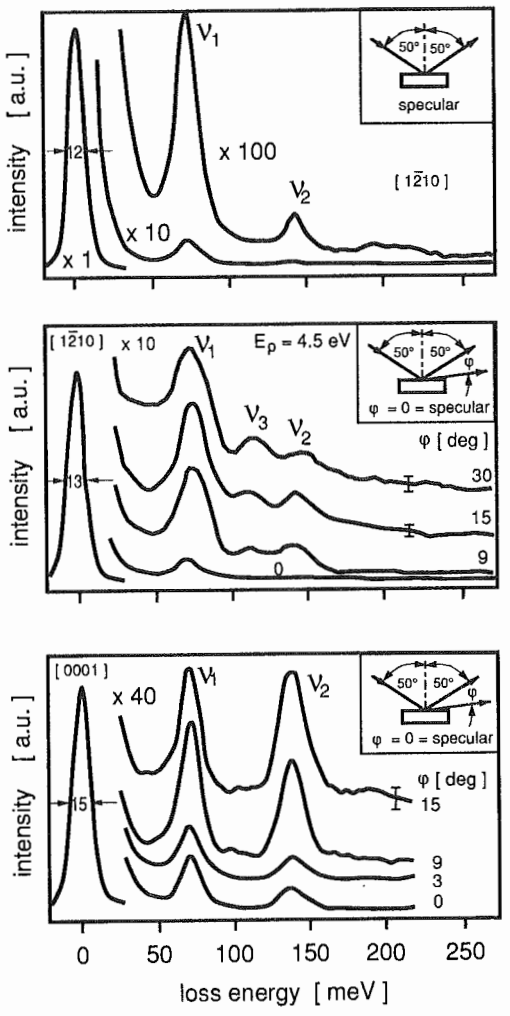

FIG. 11. (a) Vibrational loss spectrum (Ep=5.5 eV) of the (2×1)$p2mg$ structure around Θ_H=1. The spectrum was acquired in the specular direction (φ=50°) with the scattering plane directed parallel to the [1$\bar{2}$10] azimuth, i.e., along the densely packed rows. Only two losses appear under specular conditions, viz., ν_1 at 72 meV and ν_2 at 143 meV. (b) HREEL spectra of the (2×1)$p2mg$ phase (Ep=4.5 eV) acquired along the [1$\bar{2}$10] direction, however, under off-specular conditions. A third clear mode ν_3 appears around 112 meV for nonspecular scattering conditions. (c) HREEL spectra of the (2×1)$p2mg$ phase (Ep=4.5 eV) taken along the [0001] azimuth. Shown is a specular spectrum (bottom curve) and off-specular spectra. Under no conditions is the third ν_3 mode detectable.

veloped. As with the $c(2\times4)$ structure, HREEL spectra of the (transient) (2×1)$p2mg$ phase required very low hydrogen residual gas pressures and fairly fast scans which is responsible for the not too satisfactory statistics of our data. In contrast to the $c(2\times4)$ spectra, only three clear vibrational modes due to hydrogen adsorption are discernible in the loss spectra of the (2×1)$p2mg$ structure. They appear at loss energies of $\nu_1\approx71$ meV (580 cm^{-1}), $\nu_2\approx139$ meV (1118 cm^{-1}), and $\nu_3\approx112$ meV (904 cm^{-1}). In all spectra, the ν_1 mode exhibits the highest intensity which may suggest that this mode can be identified as the dipole-active perpendicular H–Co vibration. Another important feature is that the ν_3 mode is only visible when the scattering plane is aligned parallel to the [1$\bar{2}$10] azimuth [Fig. 11(b)]; if the scattering plane is rotated by 90° {parallel to the [0001] azimuth, i.e., across the densely packed rows of Co atoms, only the first two modes ν_1 and ν_2 remain visible for all off-specular angles [Fig. 11(c)]}. Conclusions on the scattering mechanism follow from the intensity variation of the elastic beam and the loss with the detection angle.[31] The count rates of the losses ν_1 and ν_2 decrease with the off-specular angle in the same way as the elastic peak, a behavior expected for dipole scattering. The ν_3 mode, however, does not show this significant drop in intensity as the detection angle deviates from the specular direction, and we attribute it therefore to impact scattering. The fact that this mode is only visible, when the scattering plane is aligned parallel to the [1$\bar{2}$10] direction requires a consideration of the symmetry selection rule for impact scattering:[31,32] if the surface is symmetric under reflection and the scattering plane is aligned parallel to the mirror plane the scattering amplitude must vanish for any scattered wave vector in the scattering plane when the mode is odd under reflection symmetry. This means that for the ν_3 mode a mirror plane aligned parallel to the [0001] azimuth must be a symmetry element of the adsorption complex, and we determine its local symmetry as C_s. Furthermore, we recall that the existence of a mirror plane along the [0001] direction implies that the (2×1) structure belongs to the $p2mg$ (and not to the $p1g1$) space group of the two-dimensional lattice. The overall existence of only three vibrational modes for the (2×1) structure is in line with the assumption that the H atoms exclusively occupy identical adsorption sites in the (2×1) structure. A similar conclusion was reached by Voigtländer *et al.*[32] who investigated the vibrational modes on a Ni(110) surface among others for the (2×1)$p2mg$ and (1×2) hydrogen phases.

3. HREELS for Θ_H>1 ML: The (1×2) phase

HREEL spectra of the (1×2) structure, obtained for coverages close to saturation (Θ=1.5) at 100 K, were taken with the scattering plane being oriented parallel to the highly symmetric directions, i.e., [1$\bar{2}$10] and [0001], and are shown in Fig. 12. Interestingly, although a third hydrogen atom is adsorbed into the (1×2) surface unit cell and the substrate undergoes a (1×2) surface reconstruction, no major differences between the spectra of Fig. 12 and those of the (2×1)$p2mg$ structure are observed. The maximum number of observed losses is still three, indicating that all hydrogen atoms occupy adsorption sites of identical local symmetry. Again, one mode only (ν_3) is impact-active and, therefore, appears only in the [1$\bar{2}$10] direction under off-specular scattering geometry—indicating a local C_s symmetry (with respect to [0001]) of the adsorbate complex. A plot of the signal intensities vs detection angle reveals again that ν_1 and ν_2 are mainly dipole-active. Compared to the (2×1) structure, cf. Fig. 11, the loss frequencies are slightly shifted to higher values: $\nu_1\approx76$ meV (609 cm^{-1}), $\nu_2\approx122$ meV (984 cm^{-1}), and $\nu_3\approx150$ meV (1205 cm^{-1}), respectively. To confirm that all observed losses are due to hydrogen vibrations, we used deuterium for dosing and obtained the same LEED structures; these were subjected to HREELS, and we found, for all losses reported above, the expected isotope shifts to lower frequencies by factors between 1.38 and 1.42 (Fig. 13). For the (1×2) phase, the similarity of the vibrational loss spectra

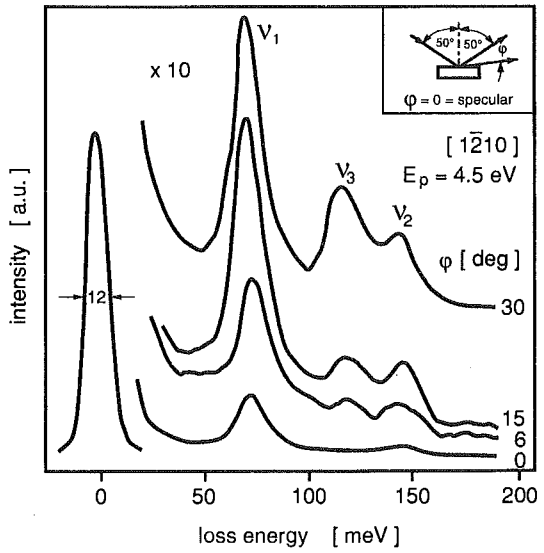

FIG. 12. HREEL spectra obtained for the (1×2) structure ($\Theta_H \approx 1.5$, Ep =4.5 eV) taken along the [1$\bar{2}$10] azimuth under specular (bottom curve) and off-specular scattering conditions. Apart from slight intensity differences, the three modes ν_1, ν_2, and ν_3 are visible, however, ν_3 only for nonspecular scattering geometry.

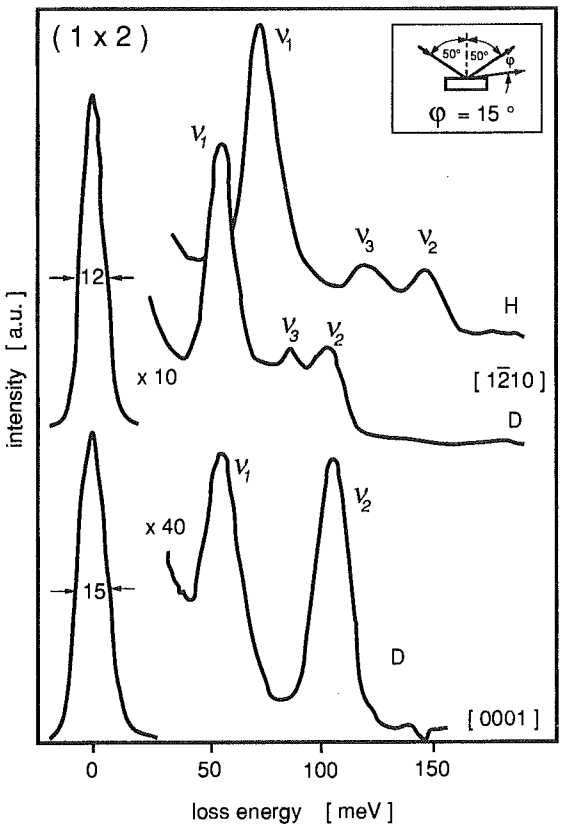

FIG. 13. HREEL spectra of the (1×2) deuterium phase which were acquired 15° off-specular parallel to the two highly symmetric directions. The D-induced bands ν_1, ν_3, and ν_2 appear at loss energies of 55, 87, and 106 MeV, respectively. When compared to the H-induced losses (top curve) these values are in good agreement with the expected isotope shift of $\sqrt{2}$.

with the preceding (2×1) structure suggests that the surface reconstruction does not affect the local geometry of the adsorption site; the additionally accommodated H atoms (half a monolayer) then must be located in the surface on geometrically still identical sites.

IV. DISCUSSION

The (dissociative) chemisorption of hydrogen on a Co(10$\bar{1}$0) surface at temperatures between 100 K and room temperature is characterized by the formation of commensurate ordered H phases in the coverage range $0<\Theta<1$, and by a reconstructive phase transformation to a (1×2) phase at higher coverages. The complete information about this system contains the energetics and kinetics of the adsorption process, the local geometry of the individual H–Co chemisorption complexes, the degree of long-range order as a function of coverage and temperature, and, finally, the development of realistic structure models, especially for the reconstructed state. In this section, we may benefit from the extensive data body that has been accumulated for cobalt's congener, the Ni(110) surface and its interaction with hydrogen, and we will, hopefully, be able to demonstrate both the similarities and the difference between these two surfaces.

A. The energetics of the H adsorption

Molecular hydrogen usually adsorbs dissociatively on transition metal surfaces; at temperatures above, say, 80 K this process takes place spontaneously, which means that the energy gain due to the adsorption (formation of two individual metal–H bonds, $E_{\mathrm{Me-H}}$) surmounts the energy requirement for the dissociation of the molecule E_{diss}. The net energy gain appears as heat of adsorption, E_{ad}, and the energy of a single metal–hydrogen bond can be calculated according to the balance

$$E_{\mathrm{Me-H}} = \tfrac{1}{2}(E_{\mathrm{diss}}^{\mathrm{H_2}} + E_{\mathrm{ad}}).$$

Cobalt behaves here completely analogous to other transition metal surfaces, and with $E_{\mathrm{diss}}=432$ kJ/mol and $E_{\mathrm{ad}}\approx 80$ kJ/mol (as it came out from the TPD and the $\Delta\Phi$ measurements) we arrive at a H–Co bond energy of approximately 256 kJ/mol (61.1 kcal/mol or 2.65 eV/bond) which agrees very well with the corresponding data obtained for Ni, Fe, Ru, Rh, or Pd.[4] We may therefore conclude on a completely analogous quantum-chemical bonding mechanism also on cobalt. With regard to the face specificity we note that similar values were also obtained in previous studies for polycrystalline cobalt[6,8] and for the basal Co plane, the (0001) surface.[9] Therefore, the (10$\bar{1}$0) surface orientation seems to exhibit the same hydrogen binding energetics as the (0001) orientation, and we do not have any hint to a particular face specificity of the H adsorption on cobalt. Quite remarkably and somewhat in contrast to Ni(110),[30] we could not detect a coverage dependence of the adsorption energy up to one monolayer, whereby the absence of such an effect is especially significant in the very low coverage range: For the Ni(110)/H system, attractive lateral H–H interactions led to

an initial increase of E_{ad} with Θ;[11,30] however, no such effect could be found with Co(10$\bar{1}$0) under similar conditions. Unfortunately, the energetics can be followed with much less accuracy in the coverage regime $\Theta>1$ monolayer, as the H-induced reconstruction is involved, and isosteric heat measurements could not be performed using the H-induced work function change due to the ambiguity of reconstruction- and adsorption-induced $\Delta\Phi$. However, the TPD results (α state!) indicate that the overall heat of adsorption is considerably lower in this range, viz., amounts to merely ~60 kJ/mol; whereby the energy reduction may be attributed to (i) the energy for the displacement of the Co atoms, and (ii) the weakening of the individual H–Co bond by repulsive lateral H–H interactions as the nearest-neighbor distances shrink. As compared to the situation of the Ni(110)/H system in the same temperature/coverage range the major difference here is that the rate of the reconstructive phase transformation (2×1)→(1×2) is (although only slightly) thermally activated in the case of Co, but occurs with Ni(110) practically spontaneously. Furthermore, there occurs a second reconstructive phase transformation with the Ni(110)/H system as the low-temperature reconstructed (1×2) phase transforms to a merely one-dimensionally ordered streak phase around 220 K;[24,33] no such phase transition could be detected with Co(10$\bar{1}$0)/H.

B. The kinetics of the H_2 adsorption

Turning to the kinetics of adsorption, we recall that there appear three different regions with different sticking probabilities. In the coverage range $0<\Theta_H<0.6$ there is a very high and practically constant probability (close to unity, within the limits of accuracy) of molecular hydrogen to stick and adsorb on Co(10$\bar{1}$0). This behavior is evidence that the dissociative adsorption takes place from a molecular precursor state. The H_2 molecule is trapped in a weak potential close to the surface but still posseses enough mobility until it has found an empty adsorption site. As the ordered $c(2\times4)$ phase is filled, s drops which means that due to the occupation of about 60% of the available adsorption sites the precursor lifetime for a H_2 molecule is too short in order to search equally successfully for an empty site. The described behavior is also very similar for hydrogen on other transition metal surfaces: high and constant sticking probabilities were reported also for H on the (110) surfaces of Ni, Pd, Rh, and Ru(10$\bar{1}$0).[4,11] However, on Co(0001), Bridge and co-workers reported, from TPD measurements, on a value of s_0 of merely 0.045, for dissociative H_2 adsorption at 300 K.[9] Although lower temperatures may lead to a somewhat larger effective sticking probability (because the rate of desorption decreases), it is a fairly general trend that the dissociative hydrogen adsorption occurs on the densely packed surfaces with much lower probability: examples are the (111) surfaces of Ni, Pd, and Pt, where s_0 is often below 0.1 pointing to a non-negligible activation energy barrier for dissociative adsorption.

After completion of the closed-packed (2×1) structure and with the onset of the reconstruction, the sticking coefficient drops to a very low value (few percent of the initial value only). A similar although somewhat less dramatic decrease was observed with the system H/Ni(110) at 120 K, again coinciding with the onset of a (1×2) reconstruction beyond $\Theta_H=1$.[24,34] It appears as if the reconstruction leads to a much less corrugated surface which provides less effective dissociation sites for the hydrogen molecule or, for some reason, introduces a new small activation energy barrier for the adsorption to take place. In Sec. III A we have determined the height of this barrier to be approximately a few kJ/mol only; nevertheless, it may substantially influence the rate of H adsorption and/or reconstruction. This imposes the question of how the combined reconstruction/adsorption occurs.

C. The mechanism of the (1×2) substrate reconstruction

We have seen that for coverages $\Theta_H>1$ a combined adsorption/reconstruction process results in the formation of a (1×2) phase which, at saturation, cf. $\Theta_H=1.5$, contains three H atoms per unit cell. From the temperature dependence of the LEED and TPD phenomena it turns out that the (1×2) phase forms as soon as the local coverage exceeds the value $\Theta_H=1$, regardless of whether the hydrogen layer is in the (2×1) ordered or in the disordered form. In the low-temperature regime, we can adjust the coverage conditions such that the (2×1) and (1×2) phases coexist. Therefore, the reconstruction can be described by a nucleation phenomenon of the "first-order" type; once the (1×2) nuclei are formed by homogeneous nucleation, the (1×2) structure starts to grow in islands at the expense of the (2×1) phase. At this stage, the LEED patterns are somewhat streaky with respect to the [1$\bar{2}$10] direction, and we conclude that the (1×2) islands grow preferentially in the direction parallel to the densely packed Co rows.

A consideration of the reconstruction mechanism must also address the question whether the dissociative adsorption alone, or the (1×2) reconstruction (with subsequent dissociative H adsorption), i.e., the displacement of the Co surface atoms, is rate-limiting and therefore responsible for the observed activation barrier. However, with our experimental means it is relatively difficult to resolve this problem, and our conclusions here must remain fairly indirect. The very low sticking probability of hydrogen for $\Theta_H>1$ could suggest that the reconstruction must occur first, before the H_2 molecules can dissociate and adsorb as atoms in the new sites generated by the reconstructed surface. The filling of the α-TPD state [which is directly associated with the (1×2) phase formation] depends linearly on the hydrogen gas pressure and occurs faster at higher surface temperatures (as long as the desorption is still negligible). We can assume that the accommodation of the hydrogen gas (which is at room temperature) to the (much lower) surface temperature is a very rapid process and occurs probably in the short time interval when the hydrogen molecule is trapped in the mobile precursor state. Since the mobility of the chemisorbed H atoms is very high even at 100 K the surface migration of the H atoms is certainly fully excited, whereas the displacements and shifts of the Co atoms apparently require a measurable activation energy. Another support for the idea that the reconstruction is rate-limiting arises from the consideration of the

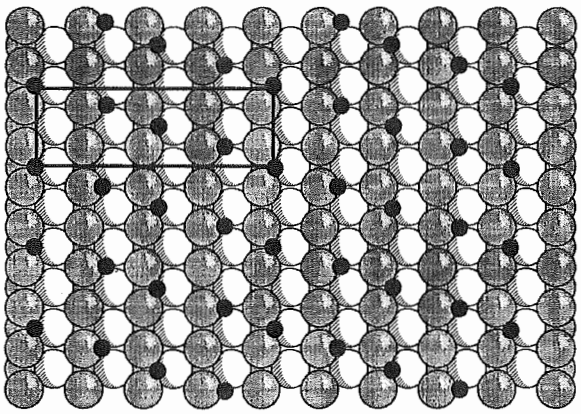

FIG. 14. Tentative structure model for the $c(2\times4)$ 4H phase on Co(10$\bar{1}$0) formed at $\Theta_H=0.5$. The H atoms are located in threefold-coordinated sites of hcp and fcc character in a way that a very homogeneous arrangement is achieved. The $c(2\times4)$ unit mesh is indicated. The Co atoms at the different height levels are indicated by shading; the H atoms are represented by the small full circles.

reverse step, namely the combined decomposition of the (1×2) reconstructed phase ("lifting" of the reconstruction) and the desorption of the α state. The maximum of the α state at 250 K is not coverage-dependent and is about four times narrower (FWHM) than the β peak (which clearly reflects associative H_2 desorption). Therefore, the rate-determining step here is not the recombination of two H atoms, but very likely the lifting of the reconstruction. When we assume the principle of microscopic reversibility being valid then also the formation of the (1×2) reconstructed phase should be rate-limiting during the adsorption reaction. After desorption of just the hydrogen fraction necessary to induce the reconstruction the substrate structure becomes (1×1) again. On Ni(110) and Pd(110) the situation with the (low-temperature) H-induced (1×2) reconstructions is relatively similar (although the activation energies to form the reconstructed phases are considerably smaller, as discussed before).

D. The structure of the ordered hydrogen phases

The ultimate goal here is certainly the complete structure analysis of all chemisorbed H phases on the Co(10$\bar{1}$0) surface, including the substrate atom positions. While a fully quantitative structure analysis has not yet been carried out we have, nevertheless, several pieces of information from LEED, HREELS, and TPD which enable us to derive tentative structure models describing both the long-range order of the H phases and the local adsorption symmetry of the individual H–Co adsorption complex.

1. The c(2×4) structure

Combined LEED and TPD studies clearly revealed an absolute hydrogen coverage of $\Theta_H=0.5$ in the $c(2\times4)$ structure; in addition, the comparatively weak extra LEED intensity suggested the absence of a major surface reconstruction. The situation for the $c(2\times4)$ structure is depicted in Fig. 14. The overall hydrogen coverage of $\Theta_H=0.5$ demands that the $c(2\times4)$ unit cell contains four H atoms and not two (as it would be true for a "primitive" cell geometry with $\Theta_H=0.25$). We recall that on most transition metal surfaces H atoms prefer sites with a high local coordination.[4] On a surface with twofold symmetry [fcc (110) and hcp (10$\bar{1}$0) face orientation], the sites with the highest coordination are quasi-threefold coordinated. There exist two kind of sites: one type consists of two Co atoms of the top layer and one Co atom of the second layer (=tetrahedral or "hcp-type" site), the other one is formed by one top-layer atom and two second-layer atoms (=octahedral or "fcc-type" site). A very similar situation is encountered with the chemically similar Ni(110) surface, where also a $c(2\times4)$ 4H phase is formed at $\Theta_H=0.5$.[24] However, in contrast to Co(10$\bar{1}$0), threefold coordinated sites with identical local symmetry, viz., the hcp-like sites, are occupied by hydrogen resulting in zig–zag rows along the [1$\bar{2}$10] azimuth. With Co(10$\bar{1}$0) on the other hand, the $c(2\times4)$ phase revealed four vibrational bands. We note that the number of observable modes depends not only on the local symmetry of the adsorption site, but also on how many hydrogen atoms are adsorbed within the unit cell in identical adsorption sites. One can then build symmetric and antisymmetric combinations which are even and odd under the symmetry operation connecting both atoms. In our case there exist four H atoms within a single unit cell, and one could expect a quadrupling of the excitable modes. However, in the case of negligible H–H interactions and infinite cobalt substrate mass (which is likely fulfilled here) these modes are fourfold degenerate. Under these conditions the observed loss features can be better reconciled with the simultaneous occupation of two adsorption sites of different local symmetry. The easiest way to distribute four H atoms in sites with a different (but high) local coordination within a $c(2\times4)$ unit cell is shown in Fig. 14—actually, both types of threefold coordinated sites (hcp-like) and (fcc-like) are occupied. The resulting (tentative) structure model is characterized by a fairly homogeneous distribution of H atoms (in diagonal rows) across the surface. Further information on the local site symmetry can be obtained by considering the HREELS impact selection rules (cf. Sec. III D). Both the hcp- and the fcc-like sites possess only a mirror plane in the [0001] direction; they are clearly of C_s symmetry. Therefore, if the scattering plane is parallel to the [0001] direction, i.e., to the mirror plane, any impact-active vibrational mode perpendicular to the mirror plane cannot be detected. This means that one would, under off-specular conditions, only expect two vibrational modes in the [0001] direction, while with the scattering plane being perpendicular to the mirror plane ([1$\bar{2}$10] direction), all three impact-active modes should be visible. Independent of these impact selection rules dipole excitation occurs; since this kind of excitation has a strong cross section only for specular geometry, it should be possible, at least in principle, to separate impact-active losses from dipole-active losses simply by choosing off-specular scattering conditions. Since for both the hcp and the fcc sites the mirror plane is aligned parallel to the [0001] direction one would expect only two pairs of impact losses when the (off-specular) scattering plane is parallel to the [0001] azimuth, but two triples of losses in the perpendicular [1$\bar{2}$10]

direction (always provided that the different site symmetry produces losses at different energies). Unfortunately, our insufficient signal-to-noise ratio did not allow a clear distinction of all these losses. Taken everything together, our observations support the simultaneous occupation of the two types of threefold coordinated sites; they are not compatible with sites of C_{2v} or C_1 symmetry (for which we skip the respective discussion of the impact scattering selection rules). It may be useful to add here that on the (hcp) Ru(10$\bar{1}$0) surface a very similar situation was encountered for a H coverage of 2—in this (1×1) 2H phase both types of threefold sites were occupied, and owing to the high density of H atoms the respective losses appeared quite clearly in the HREEL spectra.[35]

The relatively poor quality of the vibrational data of the $c(2\times4)$ phase is also the reason why we do not attempt an assignment of the various losses—it is very hard to invoke arguments which mode is the perpendicular dipole-active mode and which are the nondipole-active parallel modes; we take up this question again in the discussion of the (2×1) structure.

2. The p2mg(2×1) structure

As the H coverage reaches $\Theta_H=1.0$, the $(2\times1)p2mg$ phase dominates. The vibrational loss data suggest the occupation of only a single type of adsorption site. Analogous to the (2×1) phases formed by hydrogen on the Ni(110)/H and Pd(110)/H surfaces,[11] a very likely way to arrange the H atoms in threefold coordinated sites is the formation of adjacent zig–zag rows of H atoms in the [1$\bar{2}$10] direction, whereby this site could either be the tetrahedral hcp or the octahedral fcc site. As with the $c(2\times4)$ structure both these sites have a local C_s symmetry, i.e., they possess a mirror plane in the [0001] direction; in addition, there exists a glide-mirror plane within each zig–zag row in the [1$\bar{2}$10] direction. Both possibilities are indicated in the structure model of Fig. 15. The following considerations may help to make a decision here: For Ni(110)/H the structure of the (2×1) $p2mg$ phase was resolved by a dynamical LEED analysis[25] and by He diffraction,[26] and the hcp-like configuration [Fig. 15(A)] could be confirmed. However, care has to be taken if one adopts this structure also to the Co(10$\bar{1}$0) surface, because this is a hcp surface and exhibits somewhat different interatomic distances. LEED analyses of the uncovered Co(10$\bar{1}$0) surface revealed that the termination "A" (cf. Fig. 1) prevails. Due to the lower corrugation of this termination the distance between the first and second layer atoms is much smaller for Co(10$\bar{1}$0) ($\Delta_{12}^{Co(10\bar{1}0)}=0.72$ Å) than for Ni(110) ($\Delta_{12}^{Ni(110)}=1.14$ Å). While the distance between the metal atoms within the densely packed rows (Co: 2.507 Å; Ni: 2.492 Å) is relatively similar, the distances between the rows differ strikingly [Co(10$\bar{1}$0): 4.071 Å; Ni(110): 3.52 Å]. In a complete hydrogen layer at $\Theta_H=1$ the interatomic H–H distances are, therefore, somewhat larger on Co(10$\bar{1}$0) than on Ni(110), and the lateral H–H interactions should be less pronounced. From the already cited LEED analyses it turned out that the layer distances (also between the second and third layers) may play a crucial role to establish the most favorable adsorptive binding conditions. In this respect we

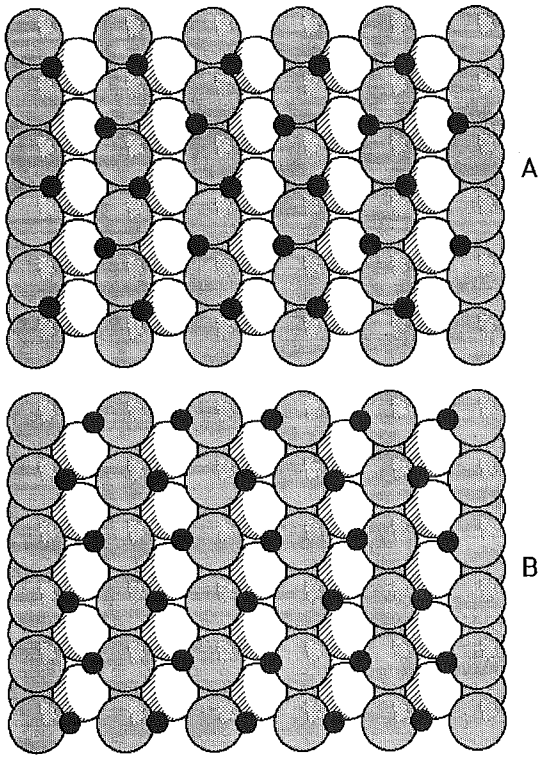

FIG. 15. Structure models for the $(2\times1)p2mg$ hydrogen phase formed on Co(10$\bar{1}$0) at $\Theta_H=1$. In configuration "A" (shown in the upper part) the H atoms exclusively occupy hcp-like sites consisting of two row atoms (dark) and one trough atom (light); in configuration "B" (shown in the lower part) only the fcc-like site (consisting of one row atom and two trough atoms) are filled. In both configurations A and B zig–zag chains of H atoms are formed along the [1$\bar{2}$10] azimuth with a glide mirror plane in the same direction.

recall that the stacking sequence for Ni (A...B...C...A...) and Co (A...B...A...) is different, and concerning the interstices, the situation on fcc (110) (Ni) is reverse to hcp (10$\bar{1}$0) (Co) with the consequence that the hydrogen atoms in the Ni(110) $p2mg(2\times1)$ structure are located above octahedral interstices. If, for quantum-chemical reasons, this type of coordination would play an important role for the H-substrate complex, one ought to favor the fcc-type of site [Fig. 15(B)] for the $(2\times1)p2mg$ phase on Co(10$\bar{1}$0). However, all in all, we do not have convincing arguments in favor of the one or the other possibility, and we must leave the decision open until more detailed structural information is available (He diffraction or dynamical LEED analysis).

As far as the assignment of the observed vibrational loss features of the $(2\times1)p2mg$ phase is concerned we recall the difficulties of such an assignment when one deals with hydrogen adsorbed layers. The normal way is to assign the most intense (dipole-active) loss to the perpendicular stretching vibration (ν_1 mode). Unlike other adsorbates this assignment is not so straightforward for hydrogen. It turns out from our structural considerations that a threefold-coordinated site is occupied by hydrogen which is somewhat inclined with respect to the surface plane; it rather represents a kind of a facet site on the scarp of a trough. Therefore, two of the three vibrational components have a perpendicular contribution and should, therefore, be dipole-active (which is indeed ob-

served for the ν_1 and ν_2 mode). We believe that ν_1 and ν_2 are the dipole-active perpendicular and parallel modes, respectively, whereas ν_3 is the nondipole-active parallel mode.

3. The reconstructed (1×2) 3H phase

We have, in the results part, given a number of arguments why we believe that the (1×2) phase is reconstructed. Taken this as granted we have the principle difficulty here that a complete structural description of the (1×2) phase involves the determination of both the structure of the reconstructed Co surface and the structure of the hydrogen adsorbed layer in or on top of the (1×2) reconstructed Co phase. Fortunately, there exist a number of structural solutions for other (1×2) reconstructed metal surfaces of twofold symmetry (for a summary, see Refs. 4 and 11) which could guide us in this question. However, among all structural solutions there is so far no hcp $(10\bar{1}0)$ surface, and we will, in the following, emphasize the peculiarities of a (1×2) reconstructed hcp surface. The most common reconstructions that occur with surfaces of twofold symmetry are of the "pairing row" (PR) and the "missing row" (MR) type. Both types of reconstructions were confirmed for hydrogen on Ni(110), the pairing row structure describing the low-temperature (90–220 K) reconstructed phase[36] and the missing row structure associated with the room temperature reconstructed phase.[37] H-induced (1×2) reconstructions were also observed for Pd(110) (PR),[38] Cu(110) (MR),[39] and Ag(110) (MR).[40] Concerning the energy requirements for the reconstructions it always turned out that the displacive reconstruction of the PR-type (which does not involve diffusion of atoms) did not require measurable activation energies, Pd(110) and low-temperature (LT)–Ni(110) being examples. On the other hand, MR reconstructions with their massive material transport requirements usually exhibit noticeable activation energies of more than 50 kJ/mol. In this respect, the quite small activation energy of 2.5 kJ/mol found with Co could perhaps point to a displacive (PR) reconstruction, but this is by no means a finite conclusion, and we will, in the following, consider both a PR and a MR reconstructed substrate surface.

Suggestions for (1×2) reconstructed surfaces are shown in Figs. 16 and 17, with the (1×2) unit cells being indicated. If we first consider a possible (1×2) missing row reconstruction, cf. Fig. 16, every second close-packed row of cobalt atoms is removed. However, in contrast to the MR reconstruction of a fcc (110) surface, the third-layer atoms are collinear with the second-layer atoms, and if we scrutinize this reconstructed surface with respect to possible hydrogen adsorption sites we find, in the upper part of the wedge-shaped trough, threefold-coordinated sites of the fcc-type, and close to the bottom of the troughs sites with a quasi-fourfold coordination. The occupation of these sites, however, should lead to different loss frequencies in our vibrational experiments, unless the H atoms located deep in the troughs are screened against low-energy electron excitation. We rule out this possibility, because such a "subsurface" hydrogen atom may be screened in a way that particularly the dipole-active modes should be selectively suppressed, but its impact-active modes will probably still be excitable. On the Ni(110) (1×2) PR phase the vibrational contributions

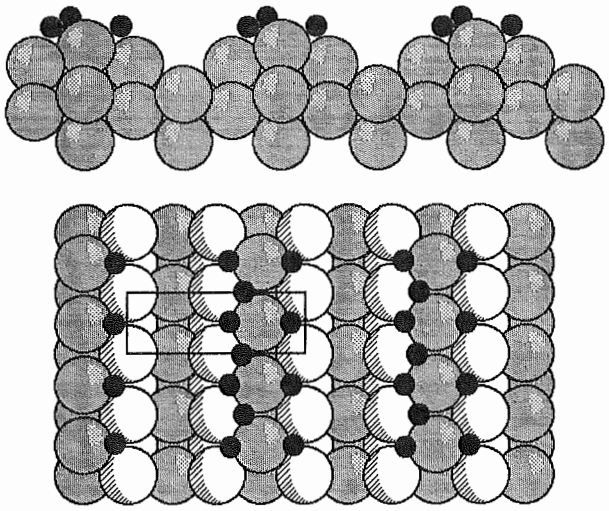

FIG. 16. Structure model suggestion for a (1×2) missing row (MR) reconstructed Co$(10\bar{1}0)$ surface covered with 1.5 monolayers of hydrogen atoms (including the side view showing the corrugation). The H atoms are filled in so as to exclusively occupy threefold-coordinated sites of the hcp and fcc type.

of the additional H atoms within the unit cell could be clearly detected, the more so, since they occupied adsorption sites which differed from the ones of the preceding (2×1) phase. Therefore, if a MR (1×2) reconstruction really occurs, all three H atoms of the (1×2) unit cell must be accommodated in the threefold sites near the upper part of the trough, with the consequence that all the respective sites are occupied by

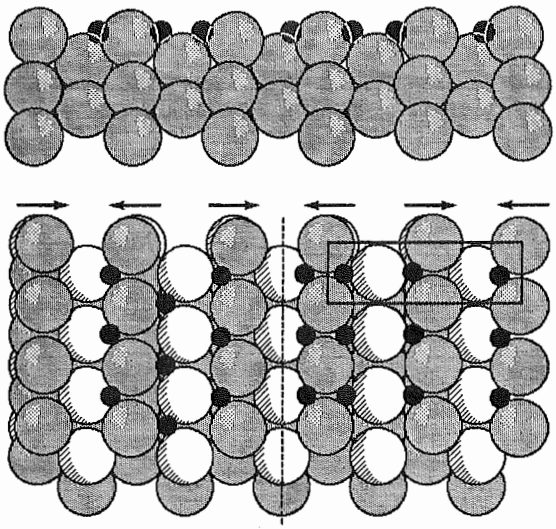

FIG. 17. Structure model suggestion for (1×2) pairing row (PR) reconstructed Co$(10\bar{1}0)$ surface covered with 1.5 monolayers of hydrogen atoms (including the side view showing the relatively small corrugation). On the left-hand part of the top view the H atoms are located in threefold sites of both hcp and fcc type, whereby a fairly homogeneous, quasihexagonal lateral distribution is attained. On the right-hand part of the figure the H atoms exclusively populate the hcp-like sites, and a relatively inhomogeneous distribution results in the [0001] direction.

H atoms—this, however, results in unphysically short H–H distances as well as in a very inhomogeneous lateral H distribution as we can see from Fig. 16 (the H atoms are indicated by the small black dots). These arguments, in particular the strong repulsive interactions between the hydrogen atoms (which are actually thought to be an important driving force for the reconstruction[41,42]) make the MR model rather unlikely. This also holds, by the way, for the so-called Bonzel–Ferrer ("sawtooth") model[43] [which likewise leads to a (1×2) reconstruction].

The pairing row (PR) model which we will discuss next leads to a much more homogeneous lateral distribution of H atoms. As shown in Fig. 17, adjacent rows of Co atoms are slightly shifted in [0001] direction against each other (indicated by arrows) in a pairwise fashion. As a result, troughs of different widths are formed, narrow ones and wide ones. This kind of reconstruction was, by the way, found to occur with the Ni(110) (1×2) LT phase, whereby the net lateral displacement is relatively small, namely only 0.4 Å, but is accompanied by a buckling of the second layer of 0.25 Å.[36] With the Co(10$\bar{1}$0) surface, we do not yet know the magnitude of the lateral (and eventual vertical) displacements (a LEED analysis is underway); at any rate, we may, for the sake of this discussion, take the creation of differently wide troughs as granted and fill in the H atoms up to a coverage of $\Theta_H=1.5$. We have, on the right-hand side of Fig. 17, depicted the possibility that the H atoms are exclusively positioned in threefold-coordinated sites of the hcp-type which results in an alternating sequence of densely packed rows of Co atoms "loaded" with double and single rows of H atoms, respectively. A perhaps more realistic situation is drawn on the left-hand part of Fig. 17: here, the H atoms occupy alternatingly hcp- and fcc-like threefold-coordinated sites and achieve a much more homogeneous lateral distribution in a quasihexagonal arrangement. Very remarkably, there is a very analog behavior reported for H on the Ru(10$\bar{1}$0) surface:[35] at $\Theta_H\approx1.3$, a (1×2) 3H phase forms with the H atoms being exclusively located in hcp-like sites. This leads to an arrangement which is, apart from the PR surface reconstruction, similar to the quasihexagonal array shown in Fig. 17. We note once more that the Ru surface does not reconstruct under these conditions, probably owing to its considerably higher cohesive energy ($E_{coh}^{Ru}=6.6$ eV; $E_{coh}^{Co}=4.39$ eV[12]). However, the Ru(10$\bar{1}$0) (1×2) 3H structure is metastable, and as the nominal coverage of $\Theta_H=1.5$ is reached, a $c(2\times2)$ phase with a somewhat larger mean H–H distance forms in which the H atoms are actually arranged in a "quasihexagonal" manner. Since, however, the substrate geometry is changed by the reconstruction, the difference between the two types of threefold sites may vanish, and a distinction via vibrational spectroscopy as on the unreconstructed surface will not be possible anymore.

ACKNOWLEDGMENTS

Financial support by the Deutsche Forschungsgemeinschaft (DFG) and the Bundesministerium für Forschung und Technologie (BMFT) is gratefully acknowledged. We thank H. Wohlgemuth for helpful discussions and K. Schubert and R. Cames for technical assistance.

[1] R. Burch, in *Chemical Physics of Solids and Their Surfaces*, Specialist Periodical Reports (The Chemical Society, London, 1979), Vol. 9, p. 309.
[2] Z. Knor, in *Catalysis*, edited by J. R. Anderson and M. Boudart (Springer, Berlin, 1982), Vol. 3, p. 231.
[3] J. W. Davenport and P. J. Estrup, in *The Chemical Physics of Solid Surfaces and Heterogeneous Catalysis*, edited by D. A. King and D. P. Woodruff (Elsevier, New York, 1989), Vol. X.
[4] K. Christmann, Surf. Sci. Rep. **9**, 1 (1988).
[5] M. A. Vannice, Catal. Rev. Sci. Eng. **14**, 153 (1976).
[6] T. Kwan, J. Res. Inst. Catal. **1**, 81 (1949).
[7] R. Culver, J. Pritchard, and F. C. Tompkins, Z. Elektrochem. **63**, 741 (1959).
[8] R. Dus and W. Lisowski, Surf. Sci. **61**, 635 (1976).
[9] M. E. Bridge, C. M. Comrie, and R. M. Lambert, J. Catal. **58**, 28 (1979).
[10] F. Greuter, T. Strathy, E. W. Plummer, and W. Eberhardt, Phys. Rev. B **33**, 736 (1986).
[11] K. Christmann, Mol. Phys. **66**, 1 (1989).
[12] K. Christmann, Z. Phys. Chem. NF **154**, 145 (1987).
[13] K. H. Ernst, E. Schwarz, and K. Christmann (to be published).
[14] M. Welz, W. Moritz, and D. Wolf, Surf. Sci. **125**, 473 (1983).
[15] H. Conrad, H. Herz, and J. Küppers, J. Phys. E **12**, 369 (1979).
[16] J. B. Hess and C. S. Barrett, J. Metals **4**, 645 (1952).
[17] P. Heilmann, E. Lang, K. Heinz, and K. Müller, in *Determination of Surface Structure by LEED*, edited by P. M. Marcus and F. Jona (Plenum, New York, 1984), p. 463.
[18] R. Unwin, W. Stenzel, A. Garbout, and H. Conrad, Rev. Sci. Instrum. **55**, 1809 (1984).
[19] H. Conrad, M. E. Kordesch, W. Stenzel, M. Sunjic, and B. Trininic-Radia, Surf. Sci. **178**, 578 (1986).
[20] H. Over, G. Kleinle, G. Ertl, W. Moritz, K. H. Ernst, H. Wohlgemuth, K. Christmann, and E. Schwarz, Surf. Sci. Lett. **254**, L469 (1991).
[21] M. Lindroos, C. J. Barnes, P. Hu, and D. A. King, Chem. Phys. Lett. **173**, 92 (1990).
[22] B. W. Holland and D. P. Woodruff, Surf. Sci. **36**, 488 (1973).
[23] M. G. Cattania, V. Penka, R. J. Behm, K. Christmann, and G. Ertl, Surf. Sci. **126**, 382 (1983).
[24] V. Penka, K. Christmann, and G. Ertl, Surf. Sci. **136**, 307 (1984).
[25] W. Reimer, V. Penka, M. Skottke, R. J. Behm, G. Ertl, and W. Moritz, Surf. Sci. **186**, 45 (1987).
[26] T. Engel and K. H. Rieder, Surf. Sci. **109**, 140 (1981).
[27] D. A. King, Surf. Sci. **47**, 384 (1975).
[28] D. A. King, Surf. Sci. **64**, 43 (1977).
[29] P. A. Redhead, Vacuum **12**, 203 (1962).
[30] K. Christmann, O. Schober, G. Ertl, and M. Neumann, J. Chem. Phys. **60**, 4528 (1974).
[31] H. Ibach and D. L. Mills, *Electron Energy Loss Spectroscopy and Surface Vibrations* (Academic, New York, 1982).
[32] B. Voigtländer, S. Lehwald, and H. Ibach, Surf. Sci. **208**, 113 (1989).
[33] K. Christmann, F. Chehab, V. Penka, and G. Ertl, Surf. Sci. **152/153**, 356 (1985).
[34] K. Christmann, in *Hydrogen Effects in Catalysis*, edited by Z. Paal and G. Menon (Dekker, New York, 1988), p. 28ff.
[35] G. Lauth, E. Schwarz, and K. Christmann, J. Chem. Phys. **91**, 3729 (1989).
[36] G. Kleinle, V. Penka, R. J. Behm, G. Ertl, and W. Moritz, Phys. Rev. Lett. **58**, 148 (1987).
[37] L. P. Nielsen, F. Besenbacher, E. Laegsgaard, and I. Stensgaard, Phys. Rev. B **44**, 13,156 (1991).
[38] H. Niehus, C. Hiller, and G. Comsa, Surf. Sci. **173**, L599 (1986).
[39] J. George, P. Zeppenfeld, R. David, M. Büchel, and G. Comsa, Surf. Sci. **289**, 201 (1993), and references therein.
[40] P. T. Sprunger and E. W. Plummer, Phys. Rev. B **48**, 14,436 (1993).
[41] G. Keinle, M. Skottke, V. Penka, G. Ertl, R. J. Behm, and W. Moritz, Surf. Sci. **189/190**, 177 (1987).
[42] V. Penka, Ph.D. thesis, University of Munich (1985).
[43] H. P. Bonzel and S. Ferrer, Surf. Sci. **118**, L263 (1982).